Rheology of Concentrated Isotropic and Anisotropic Xanthan Solutions. 1. A Rodlike Low Molecular Weight Sample

Hu-Cheng Lee and David A. Brant*

Department of Chemistry, University of California, Irvine, California 92697-2025

Received August 28, 2001

ABSTRACT: The rheology of a rodlike xanthan sample (Fraction X13F3, $M_w = 1.54 \times 10^5$ g/mol) has been studied in aqueous NaCl (0.01, 0.1, 1.0 M) in oscillatory and steady shear experiments. Polymer concentrations W (in weight percent) spanning the isotropic, biphasic, and fully anisotropic regimes of the lyotropic liquid crystalline phase diagram have been investigated. The rheological parameters increase as power law functions of W in the isotropic regime, decrease with higher power law exponents in the biphasic regime, and change very slowly in the fully anisotropic regime. The peak in plots of steady shear viscosity η against W shifts toward lower W with increasing shear rate $\dot{\gamma}$, because of the shear-induced orientation. In contrast, peaks in the plots of the complex viscosity η^*, storage modulus G', and loss modulus G'' are independent of frequency ω, because shear-induced orientation is minimal under conditions of small strain. Power law curves fit to η^*, G', and G'' in the isotropic, biphasic, and anisotropic regimes cross at W_i and at W_a, the boundaries, respectively, between the isotropic and biphasic and between the biphasic and anisotropic regions as determined by phase separation measurements. No crossover of G' and G'' is observed for X13F3 at any salt concentration studied, and the loss tangent $\tan \delta = (G''/G') > 1$ under all the conditions investigated. The parameters η^* and G'' conform to tight master curves when the appropriate reduced variables are plotted, but η and G' do not. The Cox−Merz rule is obeyed at all three salt conditions for all polymer concentrations studied in the Newtonian plateau region of the reduced flow curves. The salt concentration plays an important role in determining W_i and W_a for this ionic, rodlike polysaccharide, but it does not affect the Newtonian plateau viscosities in the isotropic regime. In contrast, the viscosities of anisotropic solutions at different salt concentrations *increase* as the salt concentration increases, because the order parameter in anisotropic solutions is greater at low salt concentration than it is at high salt concentration.

Introduction

Xanthan is a branched, ionic polysaccharide produced by the bacterium *Xanthomonas campestris*. The primary backbone is homopolymeric with repeating unit 1,4-linked β-D-glucose as in cellulose. A three-sugar side chain containing carboxyl groups is attached to every second backbone residue (Figure 1).[1,2] In aqueous solution the stable conformation of xanthan is double helical[3−5] below a transition temperature that rises from near room temperature in the absence of added salt to above the boiling point of water when the salt concentration C_s reaches 0.1 M.[6−8] The double helical chain is rather stiff with persistence length $q = 106$ nm at high salt concentration; q increases only modestly to ≈120 nm as C_s is reduced to 0.01M and is essentially independent of C_s below that salt concentration.[9] Below the transition temperature q is reported to be proportional to the inverse of absolute temperature T ($q \propto 1/T$), and the proportionality constant can be determined from the q value of 120 nm at 298 K.[10] Xanthan is widely used as an aqueous viscosity control agent owing to its high viscosity increment per unit mass and the relative insensitivity of the viscosity of the resulting solutions to salt concentration and temperature.[11]

Like many other highly asymmetric polymers, double helical xanthan forms a lyotropic liquid crystalline phase above a critical concentration.[12−14] The phase diagram has been investigated for xanthan in aqueous salt solution as a function of molecular weight at various NaCl concentrations;[15,16] see Figure 2, where xanthan concentrations c are expressed in g cm^{-3}. It displays a narrow isotropic/anisotropic biphasic region with boundary concentrations c_i between the isotropic and biphasic regions and c_a between the biphasic and anisotropic regions. For samples with narrow molecular weight distribution (MWD) both c_i and c_a approach asymptotic values as the molecular weight of the xanthan becomes great enough to make the mean contour length L of the polymer equal to about one Kuhn length, which for wormlike chains is $2q$.[16] The concentrations c_i and c_a are in the range of 0.1 g cm^{-3} at high C_s and comparable to those characterizing the lyotropic phase diagrams of neutral rigid polymers.[17] As C_s is reduced, both c_i and c_a decrease sigmoidally as electrostatic effects become prominent in the intermolecular potential.[18] Similar behavior has recently been reported for suspensions of charged cellulose crystallites.[19,20] In this paper we examine the steady shear and oscillatory rheology of a narrowly dispersed xanthan sample with $L/2q \approx 0.33$ in a polymer concentration range which spans the isotropic and biphasic regions of the phase diagram and extends into the anisotropic domain.

The phase diagram of lyotropic liquid crystalline polymers has been widely investigated, and the rheology has been of particular interest with the discovery that fibers of high tensile strength can be spun from liquid crystalline solutions of polyaramids.[21−26] An explanation of the phase separation observed in suspensions of rodlike tobacco mosaic virus was first provided by Onsager who developed the first two terms of the virial expansion for hard rodlike particles.[27] A lattice theory due to Flory permitted inclusion of variation in solvent quality.[28] Both approaches have been elaborated in

* To whom correspondence should be addressed. Telephone: +1 (949) 824-6019. Fax: +1 (949) 824-8571. E-mail dbrant@uci.edu.

10.1021/ma011526m CCC: $22.00
Published on Web 02/09/2002

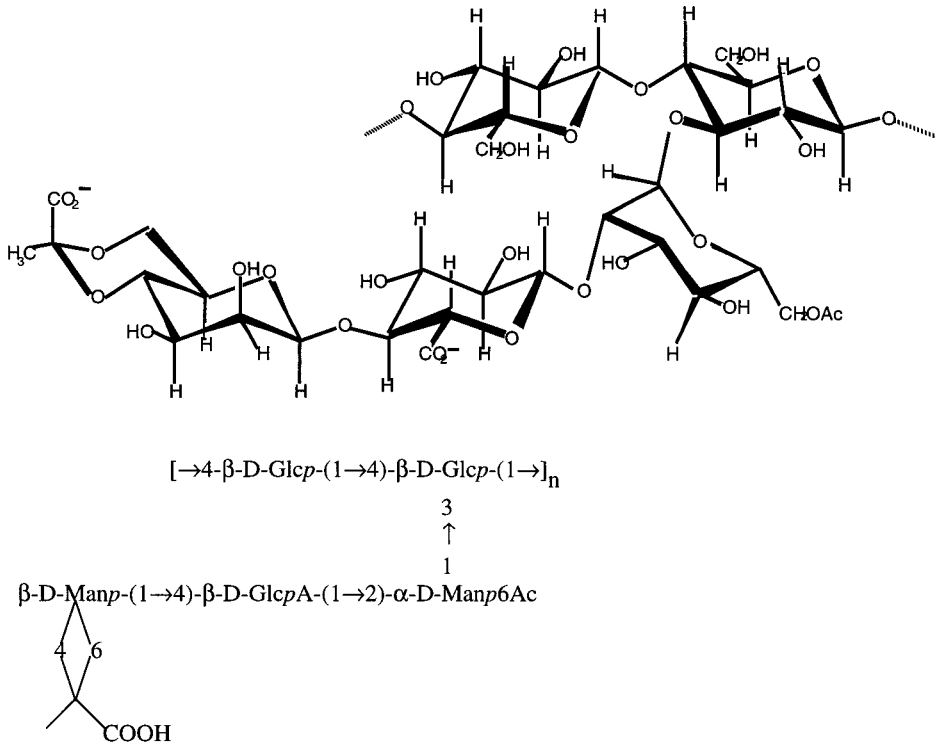

Figure 1. Repeating unit of xanthan.

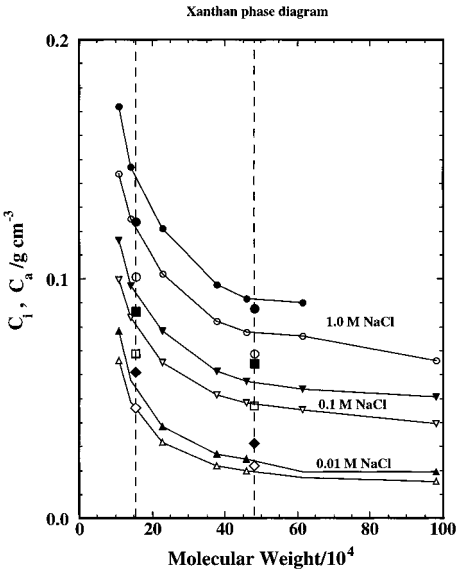

Figure 2. Molecular weight dependence of the phase boundary concentrations c_i (small open symbols) and c_a (small filled symbols) for xanthan in aqueous NaCl at concentrations C_s = 0.01, 0.1, and 1.0 M at 25 °C (constructed from the data of Inatomi et al.[16]). Phase separation results for X2F2 and X13F3 at 23 °C (larger symbols) from Figure 3; the vertical dashed lines indicate the corresponding molecular weights of these samples.

subsequent work to include the effects of polymer flexibility, molecular weight heterogeneity, and polymeric charge.[17,18,29−34] Solutions of rodlike poly(γ-benzyl-L-glutamate) were first shown by Hermans to undergo dramatic changes in viscosity as the concentration was increased into and across the biphasic domain.[35] There has been much subsequent experimental work on similar synthetic polymer systems,[36−45] and a theoretical description of the flow behavior of nematic lyotropic solutions of rodlike polymers has also emerged.[26,46−53]

The steady shear and oscillatory flow behavior of xanthan solutions has been studied extensively over a wide range of molecular weight and polymer concentration in aqueous salt solution. In the dilute regime, the dependence on molecular weight and salt concentration of the zero-shear intrinsic viscosity for double helical xanthan has been reported,[9] and the scaling of zero-shear viscosity η_0 with polymer concentration has been determined in 0.1 M aqueous NaCl for samples covering a wide range of molecular weights.[54−56] Importantly, η_0 was found to be independent of the salt concentration over the range $0.006 \leq C_s \leq 0.1$ M.[55] Most of the rheological measurements in the semidilute regime have been on unfractionated xanthan samples of relatively high molecular weight ($1-2 \times 10^6$ g/mol).[57−63] These studies show that at moderate concentrations ($W \geq \sim 1\%$) xanthan tends to form a weakly cross-linked gellike network structure that is very pseudoplastic. The cross-linking mechanism leading to this tenuous network is probably dominated by the same rather specific interactions that stabilize the double helical structure.[64] The extent to which these network stabilizing valences are present in a given xanthan sample depends on the MWD, the method of sample preparation, and, in particular, on the thermal history of the sample. Sonication and subsequent molecular weight fractionation of the double helical material produces samples with more highly perfected helical order containing fewer segments with unsatisfied double helical valency available to stabilize weak gel formation.[65,66]

A few rheological studies of xanthan have ventured into the concentration range above W_i, where the anisotropic phase first appears. Using a sample with molecular weight 2.35×10^5, Milas and Rinaudo were the first to measure the steady shear viscosity of xanthan in 0.1 M aqueous NaCl into the biphasic and completely anisotropic domains, where they observed behavior similar to that of rodlike synthetic polymers.[14] Allain et al.[67] carried out a similar, more extensive,

steady shear investigation using a high molecular weight (1.8×10^6 g/mol) xanthan sample with and without added salt and interpreted the rheology largely in terms of the Matheson theory.[46] The most extensive study of high molecular weight aqueous xanthan to date has been reported by Kulicke and co-workers, who investigated both the steady shear and oscillatory rheology of a high molecular weight sample (1.6×10^6) in 0.1 M aqueous NaCl.[68,69] Carnali attributed the characteristic weak gel behavior of high molecular weight xanthan solutions in the concentration range $W = 0.8-3.0\%$ to a dispersion of anisotropic phase within an isotropic phase.[70] Finally, Prudhomme and coworkers[71,72] have also carried out measurements on high molecular weight xanthan in the concentration range $W = 0.5-4.7\%$, which they interpret in part in terms of the presence of an anisotropic phase.

In this and subsequent papers, we report systematic investigations of the steady shear and dynamic rheology of aqueous xanthan and scleroglucan using samples that have been fractionated to yield a desired mean molar mass and relatively narrow MWD. The concentration has been varied to span the biphasic domain of the phase diagram and to probe the homogeneous isotropic and anisotropic phases on either side of the biphasic region. Measurements are reported as a function of polymer molecular weight, temperature, and, for xanthan, as a function of salt concentration. In the present paper we present the results for a low molecular weight xanthan fraction ($M_w = 1.54 \times 10^5$ g/mol, $L/2q \approx 0.33$) displaying essentially rigid rodlike behavior. These will be compared in the companion paper[73] with results on a higher molecular weight xanthan fraction ($M_w = 4.80 \times 10^5$ g/mol, $L/2q \approx 1.03$) in the asymptotic region of the curves in Figure 2. Further increase in molecular weight does not significantly affect the phase boundary concentrations W_i and W_a but does increase the absolute viscosity of the solutions making them harder to handle and impeding macroscopic separation of the phases in the biphasic domain. The present studies sample a molecular weight range quite different from that investigated by Carnali[70] and the Chauveteau[67] and Kulicke[68,69] groups.

Experimental Section

Sample Preparation. Commercial food-grade xanthan powder (Kelco Keltrol, Lot No. 76735A) was suspended in 0.1 M NaCl aqueous solution at a concentration of 9 g/L. NaN_3 was added as bactericide at concentration 0.02%. An overhead stirrer was used overnight to speed dissolution of the polymer. The resulting solution was sonicated with a Heat Systems Sonicator (20 kHz, 375 W, with 1/2 in. replaceable tip, output set at 8, duty cycle 60%) in 400 mL batches for 2 h in an ice bath. Acetone (5 mL) was added to every batch as a radical scavenger before sonication. The sonicated solution was centrifuged (Beckman Avanti J-25, rotor JA-14) at 12,500 rpm for 1 h and filtered through a 0.45 μm Millipore filter (HAWP 04700) to remove any remaining particulate matter. This process yielded a crystal clear solution, which was condensed from 4 to 2.7 L with a rotary evaporator (Büchi) to yield a clear solution with a xanthan concentration of about 13 g/L.

2-Propanol (IPA) was added dropwise to the above solution until the first appearance of white precipitate. This precipitate was collected by centrifugation at 12,500 rpm for 50 min and labeled as X2F1 (fraction 1 of 2-h sonicated xanthan). The supernatant was decanted from the precipitate, and more IPA was added to the supernatant to precipitate fraction X2F2. Fractions X2F3 (7 g) and X2F4 (discarded) were prepared by repetition of the process used to make fractions X2F1 (1.3 g) and X2F2 (19 g). Lower molecular weight fractions X13F1 (1.1 g), X13F2 (4.1 g), X13F3 (22 g), and X13F4 (4.9 g) were prepared in the same way after sonicating for 13 h. The precipitated fractions were redissolved in pure water and freeze-dried and then dried to constant weight in vacuo at 40 °C. All xanthan concentrations reported here are based on measured masses of the material vacuum-dried to constant weight at 40 °C just prior to weighing; the presence of any residual water in these samples (probably <5% (w/w)) was ignored in expressing the polymer concentration.

Table 1. Characteristics of Xanthan Samples

sample	M_w, g/mol	R_g, nm	A_2, cm^3 mol/g^2	L_w, nm	N	M_w/M_n
X2F2	4.80×10^5	83.5	4.80×10^{-4}	247	1.03	1.2
X2F3	4.22×10^5	64.2	1.15×10^{-3}	217	0.91	
X13F2	2.96×10^5	52.7	4.67×10^{-4}	152	0.63	
X13F3	1.54×10^5	37.6	4.55×10^{-4}	79	0.33	1.1
X13F4	0.628×10^5			32	0.13	

Solutions for rheological and phase volume measurements were prepared by dissolving a weighed amount of vacuum-dried xanthan fraction in ca. 5 mL of aqueous NaCl solution in a tightly capped 10 mL vial. The polymer was allowed to swell in the solvent for 1 day, and then the mixture was thoroughly agitated with a vortex mixer to obtain uniformly dispersed solutions immediately prior to loading the viscometer. Approximately 2 mL of this freshly prepared solution was transferred to a narrow test tube for observation of phase separation and measurement of the volume fraction Φ of the anisotropic phase. Polymer concentrations are expressed in weight fraction w (mass of polymer/mass of solution) or, most often, weight percent W ($100w$), but for some purposes are converted to volume fraction v (volume of polymer/volume of solution) or to concentration c (g/mL). Convenient interconversion relationships are given elsewhere.[15,74]

Characterization of Samples. The weight average molecular weights, M_w, root-mean-square z-average radii of gyration, R_g, and osmotic second virial coefficients, A_2, of X2F2, X13F3, and several other xanthan fractions were determined in 0.1 M NaCl using laser light scattering with a Brookhaven Model BI-200SM light scattering goniometer. An argon ion laser tuned to wavelength 488 nm was used as the light source. A value of 0.144 mL/g was used for the differential refractive index increment.[3] The light scattering procedures used are described elsewhere.[75,76] The measured light scattering parameters are given in Table 1 along with information on the MWD of the samples. The MWD was determined for two samples using atomic force microscopy (AFM), and from these the polydispersity index M_w/M_n was computed.[77] The weight average contour length $L_w = M_w/M_L$ (Table 1) was calculated from the measured mean molar mass and the molar mass per unit contour length M_L, 1940 g/mol nm.[4] This number is in good agreement with L_w as measured directly by AFM for samples X2F2 and X13F3. The number of Kuhn statistical segments $N = L_w/2q$, was calculated using the persistence length $q = 120$ nm, a value characteristic of xanthan in the range of salt concentrations used here.[4] Finally, the degrees of pyruvate and acetate substitution, DS_{pyr} and DS_{ace}, for the present xanthan sample were measured previously by NMR and found to be 0.59 and 0.81, respectively.[78] The polymer thus carries an average of 1.59 negative charges per repeating unit at neutral pH (Figure 1).

The dividing line between rodlike and semiflexible hydrodynamic behavior occurs at about $N = 1$,[4] and the boundary concentrations of the biphasic region of the phase diagram also become essentially independent of N above $N = 1$ as can be seen in Figure 2.[16] Data in Table 1 for the several xanthan fractions demonstrate that the fractional precipitation procedure used here is quite successful in producing fractions of different mean molar mass. Much prior experience in this lab has shown that this fractionation procedure is routinely capable of producing fractions with $M_w/M_n \approx 1.3$,[77,79] and the limited data available in Table 1 from AFM measurements confirm that the present experimental samples share this modest degree of polydispersity. Owing to the high concentra-

tions and large solution volumes required for these studies, the most abundant fractions, X2F2 and X13F3, were used, even though these are necessarily less homogeneous than a smaller fraction would be.

Rheological Measurements. Measurements were performed on a Rheometrics RFS II Fluids Spectrometer with parallel plate geometry (25 mm) using 10 and 100 g cm transducers. The respective torque ranges are 0.002−10 and 0.02−100 g cm. Most of the experiments were done using the 10 g cm transducer, except that for X2F2 in 1 M NaCl at very high polymer concentration and at high shear rates in the steady shear mode the torque was out of the range of the 10 g cm transducer. Data obtained on these samples using the 10 g cm transducer at low shear rates (up to 200 rad/s) agreed well with those obtained using the 100 g cm transducer at higher shear rates (starting from 100 rad/s), and they were fused to produce the flow curve for the specific sample. The transducers were calibrated weekly using procedures prescribed by the manufacturer; no significant drift was observed. Temperature was controlled at 23 °C with a circulating bath. Samples were loaded onto the lower plate with a spatula.

Steady shear experiments were carried out in the shear rate range $0.01 \leq \dot{\gamma} \leq 1000$ rad/s while the oscillatory dynamic experiments were done in the frequency range $0.1 \leq \omega \leq 100$ rad/s. In steady shear a delay of 10 s was applied between sequential shear rates. Some anisotropic solutions displayed overshoot or damped oscillatory stress response when the shear rate was changed. No effort was made to record such transient features, and reported measurements refer to the steady-state stress following any transients. For the oscillatory measurements a strain sweep was run prior to each frequency sweep to ensure that the strain chosen for the frequency sweep was in the linear viscoelastic regime (i.e., no dependence on strain). Strains used in the oscillatory experiments were in the range 10−120% as required to achieve satisfactory signal-to-noise ratio in the measured torque.

Parameters observed in the oscillatory measurements are the dynamic storage and loss moduli, G' and G'', respectively. From these we calculate the modulus of the complex viscosity (dynamic viscosity) $\eta^* = \sqrt{(G')^2+(G'')^2}/\omega$ and the loss tangent $\tan \delta = (G''/G')$.[80] The latter parameter measures the partitioning of the linear dynamic response between the viscous and elastic components. The Cox−Merz rule asserts that $\eta^* = \eta$ for fluids without a "structure" that can be disrupted by large strain.[81] Many of the rheological data can be plotted as reduced variables so as to conform to master curves for the data covering a wide range of concentrations. The following reduced variables were employed:[64]

$$\eta_r = \eta/\eta_0$$

$$\eta^*_r = \eta^*/\eta^*_0$$

$$G'_r = G'(M/cRT)$$

$$G''_r = (G''-\omega\eta_s)(M/cRT)$$

$$\dot{\gamma}_r = \dot{\gamma}\tau_1$$

$$\omega_r = \omega\tau_1$$

Here η_0 and η^*_0 are the viscosity and dynamic viscosity extrapolated, respectively, to zero shear and zero frequency, η_s is the solvent viscosity, M is the number average molecular weight approximated here by M_w, c is the polymer concentration in mass per unit volume, R is the gas constant, T is the Kelvin temperature, and $\tau_1 \approx \eta_0 M/cRT$ is the longest Rouse relaxation time. We obtain η_0 and η^*_0 from the measured values in the Newtonian plateau, as described below. The instrumentation reports all rheological results in cgs units, and data are plotted in conventional log−log fashion. If it is desired to convert from cgs units to SI units, 1 P = 0.1 Pa s and 1 dyn/cm^2 = 0.1 Pa.

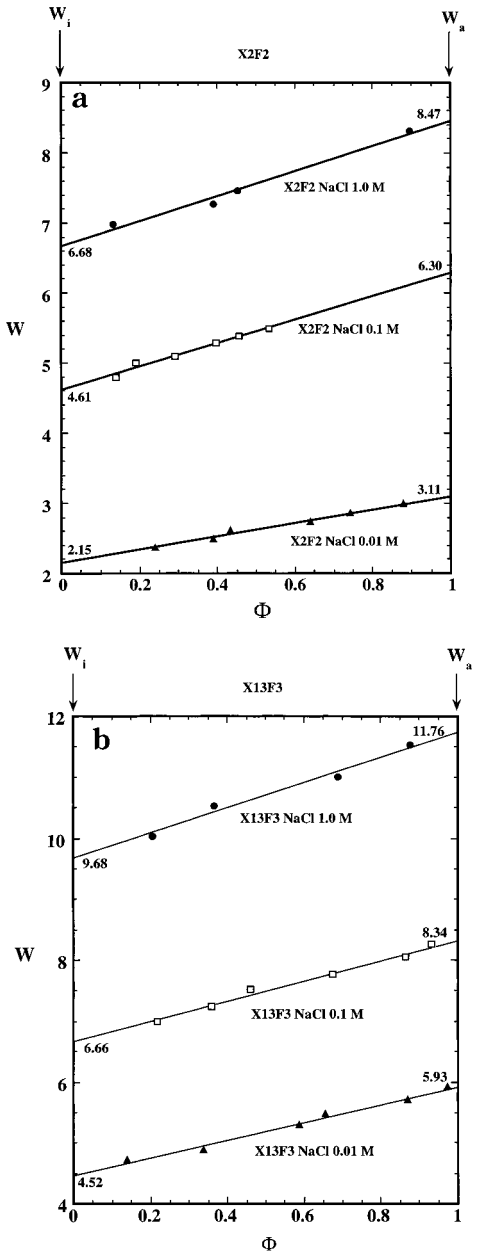

Figure 3. Overall xanthan concentration W vs the volume fraction Φ of the anisotropic phase for (a) X2F2 and (b) X13F3 in aqueous NaCl at concentrations C_s = 0.01, 0.1, and 1.0 M at 23 °C. Numbers near margins indicate W_i and W_a obtained by extrapolation to Φ = 0 and 1, respectively.

Phase Separation Measurements. In parallel with the rheological studies, all the samples were loaded into glass culture tubes (10 × 75 mm/OD × L), sealed, and subjected to centrifugation at 2500g to accelerate macroscopic phase separation in the biphasic samples. A Beckman Avanti J-25 centrifuge with JS-13.1 swinging bucket rotor was employed for centrifugation with the temperature fixed at 23 °C just as in the rheological measurements. The tubes were calibrated for measuring the volumes of the two phases. Plots of *overall* polymer weight percent W against the volume fraction Φ of the anisotropic phase permitted least squares extrapolation to the limiting weight percents W_i and W_a of the pure isotropic and anisotropic phases, respectively.[16,82] These plots are shown in Figure 3, and the values of W_i and W_a are collected in Table 2.

The approximate linearity of the plots in Figure 3 is consistent with behavior as a pseudo-two-component system, i.e., monodisperse xanthan−aqueous NaCl.[16,19,20] The lower, anisotropic, layer appears crystal clear on casual examination

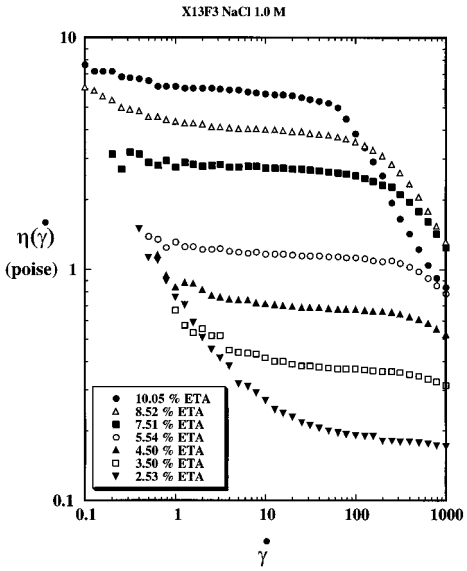

Figure 4. Steady shear viscosity $\eta(\dot{\gamma})$ for X13F3 in aqueous NaCl at $C_s = 1.0$ M vs shear rate $\dot{\gamma}$ for several solutions, most of which have $W \leq W_i$ and are fully isotropic in the quiescent state.

Table 2. Biphasic Region Boundary Concentrations

	X2F2			X13F3		
W	in 1.0 M NaCl	in 0.1 M NaCl	in 0.01 M NaCl	in 1.0 M NaCl	in 0.1 M NaCl	in 0.01 M NaCl
W_i	6.68	4.61	2.15	9.68	6.66	4.52
W_a	8.47	6.30	3.11	11.76	8.34	5.93

but is found on microscopic examination to have the "fingerprint" pattern characteristic of cholesteric liquid crystals.[17] The upper, isotropic, phase is cloudy. Comparison in Figure 2 of the c_i and c_a for samples X2F2 and X13F3 with the phase boundary concentrations measured for more narrowly dispersed xanthan fractions[16] shows that, as expected for our more broadly dispersed samples, the biphasic region of the phase diagram is broader. (Use of concentration units c_i and c_a in Figure 2 facilitates comparisons of experimental phase boundary concentrations with those obtained by application of certain theoretical models in the cited work.)[16,17] Notice also that the phase boundary concentrations of the present samples are not so highly dependent on salt concentration as those of Inatomi et al.[16] This may be because the linear charge density on our xanthan samples is smaller than that of the samples used by Inatomi et al.

Results and Discussion

Steady Shear Rheology in 1.0 M Aqueous NaCl. Figure 4 shows the steady shear viscosity $\eta(\dot{\gamma})$ of X13F3 in 1.0 M aqueous NaCl plotted against shear rate $\dot{\gamma}$ for several solutions, most of which have $W \leq W_i$ and are fully isotropic in the quiescent state. Only for the most concentrated solution ($W = 10.05$) do the data in Figure 4 intrude into the domain of biphasic quiescent solutions. All of the curves show a broad region of nearly Newtonian, behavior, as illustrated by exponent n values close to zero in Table 3; for brevity this behavior will be described simply as Newtonian in most of what follows. (We report scaling exponents n in Table 3 and elsewhere to permit ready comparison of the behavior of the systems under study here with standard viscoelastic models.) Steady shear viscosities η_0 measured approximately in the middle of the Newtonian "plateau" are reported in Table 3. All but the least concentrated solutions display shear thinning at the highest accessible shear rates. Several of the curves display a shear

Table 3. Exponent n Values for Power Laws $\eta(\dot{\gamma}) = A\dot{\gamma}^{-n}$, $\eta^*(\omega) = A\omega^{-n}$, $G'(\omega) = A\omega^n$, and $G''(\omega) = A\omega^n$, and Newtonian Plateau Viscosities η_0 and η^*_0 for X13F3 in Poise in 1.0 M Aqueous NaCl[a]

W	$\eta(\dot{\gamma})$			η_0	$\eta^*(\omega)$	$G'(\omega)$	$G''(\omega)$	η^*_0
	Low $\dot{\gamma}$	Intermed $\dot{\gamma}$	High $\dot{\gamma}$					
2.53	0.581	0.060		0.18	0.062	1.831	0.918	0.176
3.50		0.032		0.37	0.002	1.854	0.946	0.362
4.50		0.035		0.68	0.001	1.985	0.990	0.662
5.54		0.027	0.284	1.20	0.006	1.952	0.987	1.15
6.51		0.038	0.369	2.00	0.021	1.788	0.931	1.97
7.51		0.019	0.491	2.80	0.013	1.848	0.979	2.75
8.52		0.030	0.620	4.20	0.011	1.848	0.987	3.95
9.49		0.019	0.708	5.80	0.009	1.778	0.984	5.56
10.05		0.035	0.684	6.20	0.037	1.593	0.961	6.15
10.54		0.037	0.662	4.25	0.032	1.557	0.956	4.20
11.02		0.070	0.117	2.25	0.023	1.783	0.970	2.20
11.54		0.021		1.58	0.028	1.847	0.971	1.52
12.08		0.047		1.20	0.016	1.809	0.966	1.07
12.51		0.028		1.03	0.016	1.805	0.967	0.89
13.27		0.027		1.01	0.012	1.816	0.970	0.88
13.87		0.034		0.96	0.017	1.811	0.968	0.86
14.97		0.035		0.88	0.019	1.778	0.955	0.82
16.21	0.260	- 0.071	0.038	0.84	0.033	1.769	0.947	0.80
17.75	0.226	- 0.094	0.041	0.82	0.038	1.625	0.930	0.76
20.16	0.271	- 0.077	0.053	0.88	0.034	1.617	0.927	0.79

[a] Bold horizontal lines separate solutions that, when quiescent, are isotropic (top), biphasic (middle), and anisotropic (bottom). Bold vertical line separates steady shear and oscillatory data.

thinning region at low shear rates. Low shear rate shear thinning (region I) behavior is often discussed in the context of liquid crystalline polymers,[21,22,26,37,53] but to our knowledge so far only for solutions with nematic character, which is absent in the cases (e.g., $W = 2.53$ and 3.50) shown here.

The Newtonian plateau viscosity increases steadily with increasing concentration in Figure 4, as is normally observed for isotropic polymer solutions. Note, however, that the solutions of highest concentration show a reversal of this trend in the shear thinning region at high $\dot{\gamma}$. Figure 5 displays the dependence of $\eta(\dot{\gamma})$ on $\dot{\gamma}$ for X13F3 solutions of higher concentration; the curve for $W = 10.05$ from Figure 4 is repeated. In the concentration range $10.05 \leq W \leq 11.54$ the plateau viscosity *decreases* as the polymer concentration increases, because these samples contain an increasing volume fraction Φ of the less viscous anisotropic phase as the overall concentration W increases (Figure 3). The samples with $W \geq 12.08$ are fully anisotropic in the quiescent state. Further increase in the polymer concentration into the fully anisotropic domain leads to little further change in the plateau viscosity, but as the concentration reaches $W \approx 15$ shear thinning behavior emerges at low shear rates followed by a short region of shear thickening before the viscosity converges at higher $\dot{\gamma}$ to a behavior that is essentially independent of both concentration and shear rate. Under these

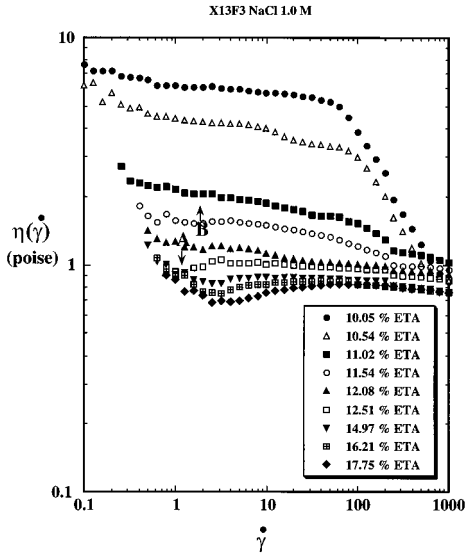

Figure 5. Steady shear viscosity $\eta(\dot{\gamma})$ for X13F3 in aqueous NaCl at $C_s = 1.0$ M vs shear rate $\dot{\gamma}$ for solutions that are in the biphasic and fully anisotropic regimes in the quiescent state. Curves above B with $10.05 \leq W \leq 11.54$ are biphasic; curves below A with $12.08 \leq W \leq 17.75$ are anisotropic.

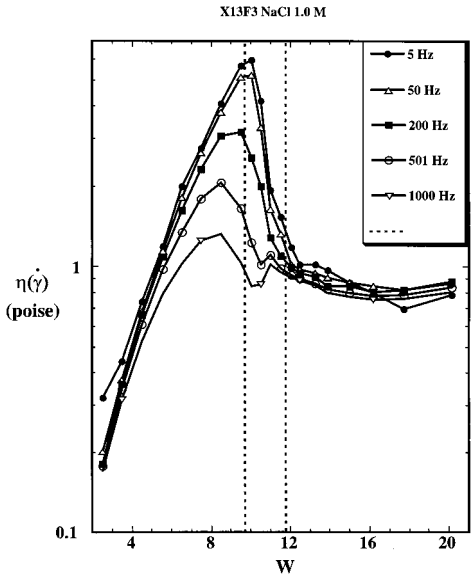

Figure 6. Steady shear viscosity $\eta(\dot{\gamma})$ for X13F3 in aqueous NaCl at $C_s = 1.0$ M vs concentration W for several shear rates; vertical dashed lines indicate the phase boundary concentrations W_i and W_a in the quiescent state.

conditions, polymer chain alignment by the shear field dominates the excluded volume and other possible interactions that account for the spontaneous liquid crystallinity of the quiescent solutions.[26,51] The shear thinning behavior at low $\dot{\gamma}$ is reminiscent of region I behavior reported earlier for nematic lyotropic polymer liquid crystals, but it occurs here in solutions much less viscous than those normally associated with region I behavior ($\eta = 1000$ P).[26] The nearly Newtonian behavior at higher $\dot{\gamma}$ appears consistent with earlier reports of the behavior of polymer lyotropic nematics in region II, but the shear thickening regime seen here at intermediate $\dot{\gamma}$ is not usually observed. The shear thinning behavior at high $\dot{\gamma}$ often observed with lyotropic nematics (region III) is apparently out of reach for X13F3 given the current maximum shear rate of 1000 s^{-1}; it appears prominently with the higher molecular weight sample described in the companion paper.[73]

The data of Figures 4 and 5 are conveniently summarized by plotting the viscosities at several fixed shear rates as a function of polymer concentration in Figure 6. Vertical dashed lines identify W_i and W_a for the quiescent solutions. The peak in these plots, which is close to W_i at low shear rate, moves to lower W as $\dot{\gamma}$ increases. The shear rate dependence of $\eta(\dot{\gamma})$ is clearly most pronounced in the concentration range close to, and below, W_i. Above W_a, $\eta(\dot{\gamma})$ becomes effectively independent of both shear rate and concentration. There are very strong dependences of $\eta(\dot{\gamma})$ on W for $W \leq W_i$ at all shear rates and for $W_i \leq W \leq W_a$ at low shear rates. A sharp increase in $\eta(\dot{\gamma})$ with W in the range below W_i is followed by an even more abrupt decline in $\eta(\dot{\gamma})$ with W across the concentration range of biphasic quiescent solutions. The special features of the biphasic region can still be observed at the highest shear rate covered. This is in contrast to the case of semiflexible xanthan for which under high shear stress there is little, if any, distinction between the isotropic and anisotropic phases, and $\eta(\dot{\gamma})$ increases monotonically with W until the chains achieve an asymptotic degree of alignment and $\eta(\dot{\gamma})$ becomes effectively independent of W.[73]

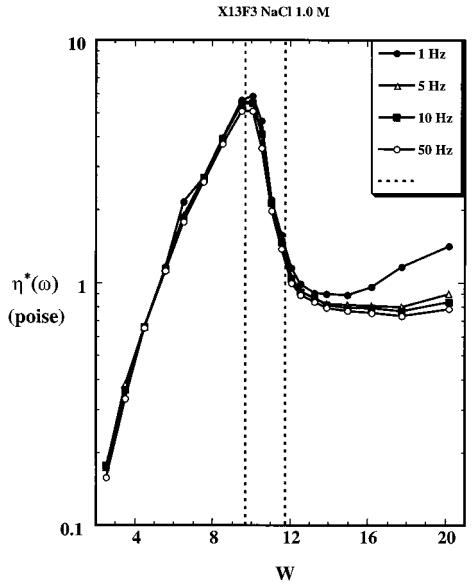

Figure 7. Oscillatory shear viscosity $\eta^*(\omega)$ for X13F3 in aqueous NaCl at $C_s = 1.0$ M vs concentration W for several frequencies; vertical dashed lines indicate the phase boundary concentrations W_i and W_a in the quiescent state.

Oscillatory Rheology in 1.0 M Aqueous NaCl. Oscillatory shear data plotted as $\eta^*(\omega)$ against ω across the concentration range $2.35 \leq W \leq 20.16$ are very similar to the plots of $\eta(\dot{\gamma})$ against $\dot{\gamma}$ shown in Figures 4 and 5, except that the shear thinning observed in some of the samples at high $\dot{\gamma}$ in steady shear is not observed because the highest accessible frequency was 100 s^{-1}. These results are summarized in Figure 7, which can be compared directly with the corresponding plot for the steady shear results in Figure 6. In oscillatory shear the maximum occurring near W_i does not change height or position as ω increases. At the lowest frequencies the decline in $\eta^*(\omega)$ which occurs on crossing the concentration domain of biphasic quiescent solutions is followed by an increase in $\eta^*(\omega)$ with W that is not observed in Figure 6 at even the lowest shear rates. These differences are clearly related to the fact that under the

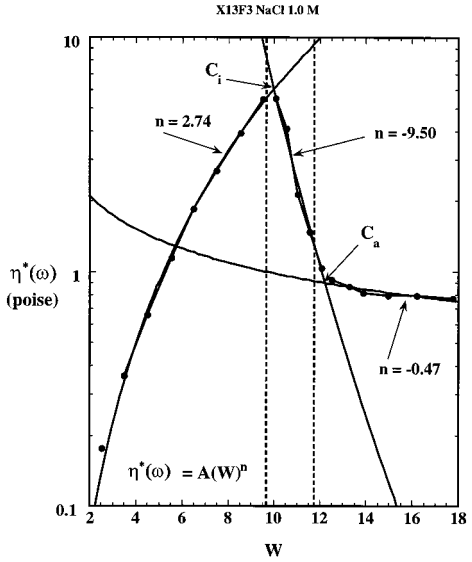

Figure 8. Demonstration of phase boundary concentration determination from power law plots of dynamic viscosity $\eta^*(\omega)$ for X13F3 in aqueous NaCl at $C_s = 1.0$ M vs W for frequency $\omega = 5$ Hz; vertical dashed lines indicate the phase boundary concentrations W_i and W_a in the quiescent state. Power law exponents n are shown for each domain of the phase diagram.

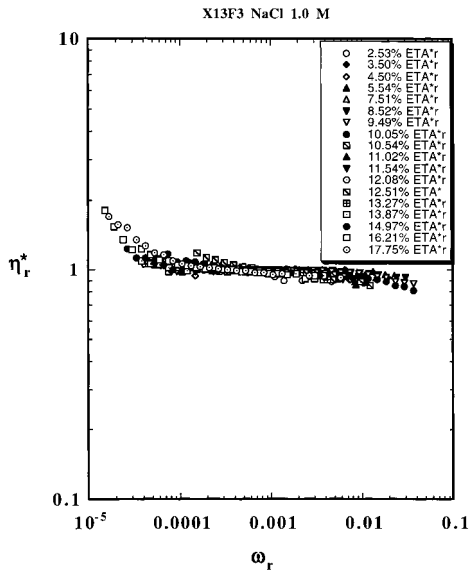

Figure 9. Master curve of reduced dynamic viscosity η^*_r for X13F3 in aqueous NaCl at $C_s = 1.0$ M vs reduced frequency ω_r, with all the solutions included.

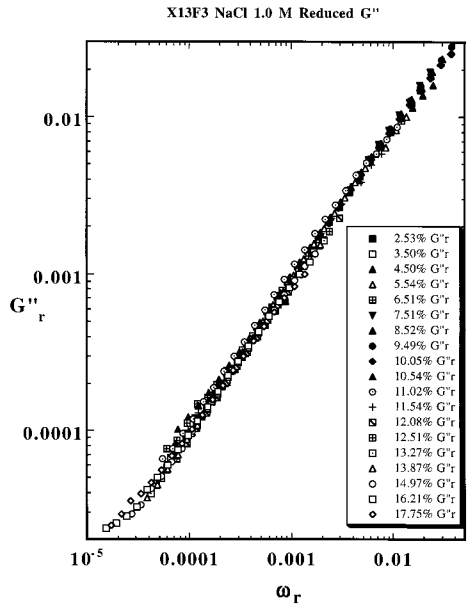

Figure 10. Master curve of reduced loss modulus G''_r for X13F3 in aqueous NaCl at $C_s = 1.0$ M vs reduced frequency ω_r, with all the solutions included.

relatively small strain conditions of the oscillatory measurements the extent of molecular alignment is much less dependent on the existence of the shear field than is the case in steady shear. This enables one to use the data in Figure 7 to identify rather accurately the concentrations W_i and W_a that characterize the concentrations of the isotropic and anisotropic phase in quiescent biphasic systems. The concentration dependence of $\eta^*(\omega)$ in each concentration domain can be accurately fit to a power law expression of the form $\eta^*(\omega) = AW^n$. It can be seen in Figure 8 that the intersections of the power law curves occur rather close to W_i and W_a. The scaling exponent $n = 2.74$ in the isotropic region is close to 3 which is expected on theoretical grounds.[47,49]

It is also useful to observe that all of the measurements of $\eta^*(\omega)$ as a function of W and ω can be brought onto a master curve by employing the reduced variables η^*_r and ω_r defined above. These results are shown in Figure 9, where it is seen that nearly all of the data fall in the Newtonian regime with just some hint of region I behavior for a few of the fully anisotropic samples. Values of η^*_0 needed to convert the data in Figure 9 to the actual values of η^* at each concentration and frequency are given in Table 3. A reduced variable approach works somewhat less well for the steady shear data. Plots of η_r against $\dot\gamma_r$ do not conform to a single master curve for those solutions that are biphasic in the quiescent state. For these solutions the texture of the fluid, and the corresponding spectrum of relaxation processes, changes both with W and with $\dot\gamma$ so that a single master curve does not result, in particular, in the higher range of $\dot\gamma$. It is interesting that, by contrast, the solutions with $W_i \le W \le W_a$ all conform well to the master curve in Figure 9. This leads to the somewhat surprising suggestion that the solutions that are biphasic when quiescent relax under oscillatory shear in ways that are very similar to the relaxation processes in the homogeneous isotropic and anisotropic fluids. In steady shear, the solutions with $W \ge W_a$ also show some deviations of η_r from the master curve in the region of small $\dot\gamma$. Despite the cited differences in the behavior of the reduced viscosities η_r and η^*_r, the Cox−Merz rule is well satisfied for solutions of X13F3 at all concentrations studied in the Newtonian plateau region of the reduced flow curves in the range $0.0001 \le \dot\gamma_r, \omega_r \le 0.05$. This can be confirmed by comparing the values of η_0 and η^*_0 in Table 3.

The loss tangent exceeds unity for nearly all of the X13F3 solutions studied here. Even at the highest accessible frequencies these solutions, whether isotropic, biphasic, or anisotropic in the quiescent state, are more viscous than elastic in their response to oscillatory shear. The plot of G''_r against ω_r in Figure 10 displays a single tight master curve embracing solutions with concentrations varying from $W \le W_i$ to $W \ge W_a$. The slope of the plot is very close to unity as is expected for polymeric fluids without significant entanglements.[80] Plots of G'_r against ω_r, in contrast, do not conform well

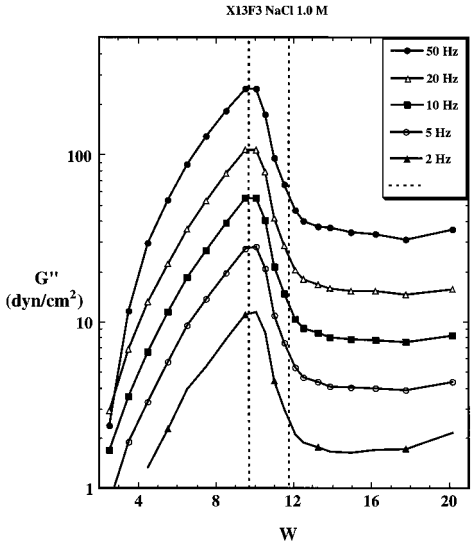

Figure 11. Loss modulus G'' for X13F3 in aqueous NaCl at $C_s = 1.0$ M vs concentration W for several frequencies; vertical dashed lines indicate the phase boundary concentrations W_i and W_a in the quiescent state.

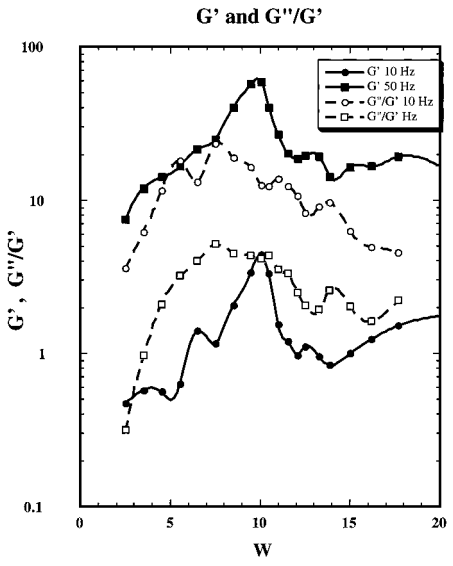

Figure 12. Plots of G' and G''/G' against W for X13F3 at $C_s = 1.0$ M for $\omega = 10$ and 50 Hz.

to a master curve. This may be a reflection of the smaller signal-to-noise ratios for measurement of G', which may be as much as 10 times smaller than G'', but in fact, we have no very satisfactory explanation for the failure of G'_r to fall on a tight master curve. The slopes of all G'_r vs ω_r curves are close to 2 as expected for polymeric fluids without significant entanglements.[80]

The explicit dependence of G'' on concentration is illustrated in Figure 11, where G'' is plotted against W for several values of ω. Vertical dashed lines identify the concentrations W_i and W_a for quiescent solutions. The plot is reminiscent of Figure 7, but in this case G'' increases monotonically with increasing ω as expected (Figure 10). The peak does not shift along the W axis with changes in ω, and it occurs very close to W_i. Plots of G' against W, shown for $\omega = 10$ and 50 s^{-1} in Figure 12, present a very similar picture, but the curves are somewhat noisier owing to the relatively large loss tangent, and the vertical relief in the line at any given ω is less than seen in Figure 11. Corresponding loss tangents G''/G' are plotted in Figure 12 to illustrate that

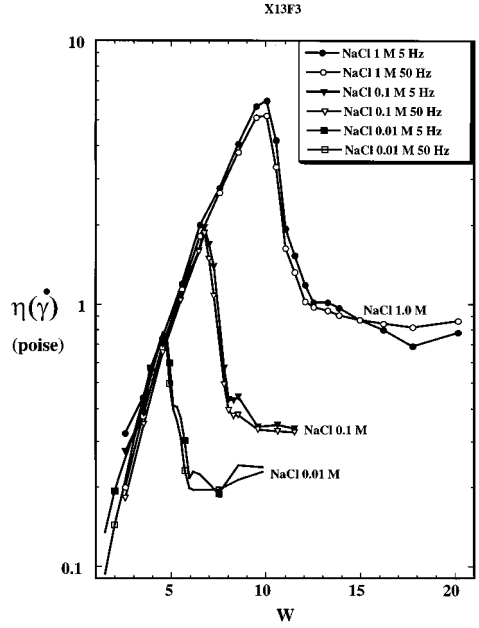

Figure 13. Steady shear viscosity $\eta(\dot\gamma)$ of X13F3 in aqueous NaCl at $C_s = 0.01$, 0.1, and 1.0 M vs concentration W for shear rates 5 and 50 Hz.

the loss tangent displays the conventional decrease with increasing ω regardless of W. The loss tangent is not monotonic with W, but there are no features in the loss tangent curves that are easily identified with passage through the biphasic domain of the phase diagram. Analogues of Figure 8 for both G' and G'' again show crossings of the several power law curves very close to W_i and W_a.

Salt Dependence of the Steady Shear and Oscillatory Rheology of X13F3. The effect on steady shear viscosity of reducing the NaCl concentration C_s to 0.1 and 0.01 M is summarized in Figure 13, where $\eta(\dot\gamma)$ is plotted against W for two values of the shear rate. The two curves at the top of this figure reproduce the top two curves in Figure 6 for $C_s = 1.0$ M, while the lower pairs of curves correspond, successively, to $C_s = 0.1$ and 0.01 M. The maxima in Figure 13 occur for W almost equal to W_i for each of the respective values of C_s (see Table 2). As the shear rate is increased above the relatively small values shown in Figure 13, the peak moves to smaller values of W as seen in Figure 6. The maximum declines in amplitude as $\dot\gamma$ increases, but persists as a distinct maximum at even the highest accessible shear rates (1000 s^{-1}) at all values of C_s. Primary plots of $\eta(\dot\gamma)$ against $\dot\gamma$ at $C_s = 0.1$ and 0.01 M are very similar to those shown in Figures 4 and 5. Only the weak shear thickening behavior shown in Figure 5 for solutions that are fully anisotropic when quiescent is absent from the corresponding plots at $C_s = 0.1$ and 0.01 M.

The salt dependence of the complex viscosity is presented in Figure 14. These data at low frequency are essentially indistinguishable from the steady shear results in Figure 13. But whereas the steady shear data show shear thinning behavior for solutions that are isotropic and biphasic in the quiescent state (see Figure 6), the oscillatory results are Newtonian regardless of the phases present in the quiescent liquid as illustrated by the exponent n values listed in Tables 4 and 5. In all respects the concentration and frequency dependences of G' and G'' resemble those of these quantities

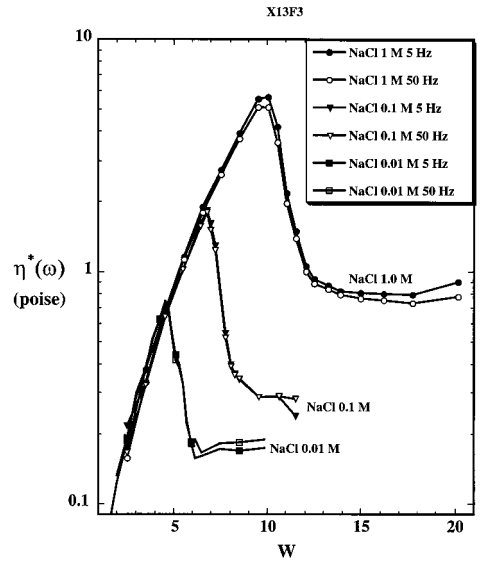

Figure 14. Dynamic viscosity $\eta^*(\omega)$ of X13F3 in aqueous NaCl at $C_s = 0.01$, 0.1, and 1.0 M vs concentration W for frequencies 5 and 50 Hz.

Table 4. Exponent n Values for Power Laws $\eta(\dot\gamma) = A\dot\gamma^{-n}$, $\eta^*(\omega) = A\omega^{-n}$, $G'(\omega) = A\omega^n$, and $G''(\omega) = A\omega^n$, and Newtonian Plateau Viscosities η_0 and η^*_0 for X13F3 in Poise in 0.1 M Aqueous NaCl[a]

W	$\eta(\dot\gamma)$			η_0	$\eta^*(\omega)$	$G'(\omega)$	$G''(\omega)$	η^*_0
	Low $\dot\gamma$	Intermed $\dot\gamma$	High $\dot\gamma$					
2.53	0.268	0.034		0.160	0.085	1.755	0.808	0.167
3.54		0.026	0.117	0.345	0.005	1.967	0.985	0.330
4.56		0.025	0.200	0.650	0.005	1.836	0.976	0.640
5.50		0.017	0.307	1.050	0.001	1.954	0.996	1.020
6.46		0.030	0.730	1.570	0.008	1.849	0.994	1.590
6.76		0.031	0.705	1.930	0.008	1.857	0.985	1.820
6.99		0.053	0.629	1.620	0.023	1.736	0.943	1.550
7.25		0.063	0.624	1.500	0.017	1.723	0.947	1.250
7.52		0.208	0.605	1.250	0.029	1.709	0.974	1.300
7.77		0.057	0.150	0.560	0.012	1.867	0.968	0.530
8.05		0.037	0.085	0.440	0.003	1.776	0.969	0.380
8.27		0.067	0.033	0.426	0.010	1.797	0.966	0.360
9.57		0.019		0.34	0.010	1.922	0.950	0.280
10.63		0.013		0.33	0.014	1.812	0.971	0.280
11.52		0.014		0.33		1.925	1.000	0.260

[a] Bold horizontal lines separate solutions that, when quiescent, are isotropic (top), biphasic (middle), and anisotropic (bottom). Bold vertical line separates steady shear and oscillatory data.

at the higher salt concentration (see the discussion of Figures 10−12).

When the reduced variable methods applied at $C_s = 1.0$ M are employed for the data at lower salt concentrations very similar results are obtained. Plots of η^*_r and G''_r against ω_r for the lower values of C_s can be brought onto master curves similar to those shown in Figures 9 and 10, respectively, for solutions that range from fully isotropic to fully anisotropic when quiescent. As is found at $C_s = 1.0$ M, η_r vs $\dot\gamma_r$ and G'_r vs ω_r do not conform to

Table 5. Exponent n Values for Power Laws $\eta(\dot\gamma) = A\dot\gamma^{-n}$, $\eta^*(\omega) = A\omega^{-n}$, $G'(\omega) = A\omega^n$, and $G''(\omega) = A\omega^n$, and Newtonian Plateau Viscosities η_0 and η^*_0 for X13F3 in Poise in 0.01 M Aqueous NaCl[a]

W	$\eta(\dot\gamma)$			η_0	$\eta^*(\omega)$	$G'(\omega)$	$G''(\omega)$	η^*_0
	Low $\dot\gamma$	Intermed $\dot\gamma$	High $\dot\gamma$					
2.00	0.130	0.022		0.132	0.023	1.825	0.970	0.130
2.52		0.032		0.196	0.015	1.970	0.960	0.189
3.03		0.029		0.299	0.001	1.887	0.989	0.295
3.49		0.026		0.383	0.001	2.000	0.984	0.380
3.87		0.024	0.237	0.516	0.005	1.970	0.988	0.515
4.25		0.018	0.405	0.634	0.005	1.908	0.985	0.625
4.54		0.019	0.666	0.752	0.001	1.993	0.994	0.740
4.72		0.038	0.634	0.770	0.039	1.931	0.955	0.710
4.89		0.027		0.585	0.047	1.813	0.948	0.550
5.09		0.037		0.420	0.038	1.759	0.946	0.430
5.30		0.062		0.410	0.013	1.910	0.967	0.390
5.49		0.061		0.340	0.022	1.895	0.978	0.330
5.71		0.086		0.280	0.002		0.976	0.226
5.92		0.033		0.220	0.009	1.881	0.970	0.180
6.12		0.029		0.200	0.007	1.921	0.971	0.170
6.50		0.024		0.200	0.004	1.997	0.974	0.160
7.47		0.004		0.200	0.004	1.890	0.970	0.170
8.52		0.023		0.220	0	1.817	0.988	0.170
9.83		0.011		0.230	0	1.862	0.992	0.180

[a] Bold horizontal lines separate solutions that, when quiescent, are isotropic (top), biphasic (middle), and anisotropic (bottom). Bold vertical line separates steady shear and oscillatory data.

master curves using the reduced variables employed here.

Finally we observe in both Figures 13 and 14 that the curves for all three salt concentrations have the same shape except for a shifting of the peak position and reduction of peak amplitude as the salt concentration decreases. What is more, the curves before reaching their respective maxima overlap with each other for all three salt concentrations. This demonstrates that the viscosity in the isotropic region is independent of salt concentration for sample X13F3, as reported by Takada et al. for the zero-shear viscosity of xanthan at several molecular weights.[55] This independence of salt concentration clearly does not extend into the concentration domain where $W \geq W_i$. Indeed, the behavior in the domain of solutions with $W \geq W_a$ that are anisotropic when quiescent is quite remarkable in that here the viscosity of the polyelectrolyte solutions *increases* as the salt concentration is increased.

It is useful here to recall that a decrease in C_s has the effect of increasing the range of the electrostatic interactions among the rodlike xanthan double helices. In these very asymmetric molecules the consequence is primarily to increase the effective diameter, since the Debye radius even at $C_s = 0.01$ M (ca. 3 nm) is much smaller than the contour length $L_w = 79$ nm of X13F3. As seen from Figures 2, 13, and 14, these changes in effective diameter strongly influence the phase boundary concentrations W_i and W_a. However, as already

remarked by Takada et al.,[55] it is clear that the electrostatic interactions between X13F3 molecules in the isotropic phase do not contribute to the solution viscosity. This is obviously because the hydrodynamic volume of the rodlike xanthan molecules in isotropic solution is insensitive to the ionic strength, in strong contrast to the behavior of flexible chain polyelectrolytes. The identity of $\eta(\dot{\gamma})$ or $\eta^*(\omega)$ for isotropic X13F3 solutions at a given W (e.g., 4%), but with different values of C_s, means that the power dissipated per unit volume in shearing the solutions at a given shear rate is independent of the effective diameters of the xanthan double helices. This is certainly a plausible circumstance, given that the axial ratios of xanthan at these two different C_s values are scarcely different.

On the contrary, when two anisotropic X13F3 solutions at a given W but with different salt concentrations are sheared at a given rate the power dissipation per unit volume is greater at the higher C_s. Stroobants et al.,[32] in extending the Onsager theory[27] to incorporate the effects of electrostatic interactions between rodlike polyelectrolytes, demonstrate that the order parameter for the anisotropic phase at $W = W_a$ increases with increasing effective diameter (decreasing C_s). Hence, it easy to understand that more power must be dissipated per unit volume to shear the less well aligned rods at high C_s than is required for the better aligned systems of lower C_s.

Conclusion

The concentration and shear rate/frequency dependences of η, η^*, G', and G'' for low molecular weight, rodlike xanthan rheology are very similar to those observed for rodlike synthetic polypeptides.[35,36,83] It does not appear that similarly extensive rheological studies have been carried out on any other rodlike polyelectrolyte, however. Changes in salt concentration have a strong influence on the phase boundary concentrations W_i and W_a, but the rheological behavior is nevertheless very similar from one salt concentration to the next apart from differences in the specific concentrations (close to W_i and W_a) at which the details of the concentration and shear rate/frequency dependences change form. The viscosity in the isotropic regime at different salt concentrations overlaps, indicating that η and η^*depend only on polymer concentration and not on salt concentration for this rigid rodlike polyelectrolyte in the isotropic phase. This is in contrast to the anisotropic solutions for which η and η^* *increase* with increasing salt concentration, behavior that is highly unusual for a polyelectrolyte. Except for differences in the *range* of the excluded volume interactions leading to spontaneous ordering of quiescent xanthan solutions at different salt concentrations, behavior in the several salt concentrations studied here is very similar. Absence of any crossover in plots of G' and G'' against ω and adherence to the Cox−Merz rule throughout the accessible range of ω imply that long-lived entanglements with relaxation times $\tau \geq 0.01$ s are absent in these rather concentrated systems of rigid rods. The wormlike sample X2F2 described in the following paper is different from X13F3 in this respect.[73]

In this context it is interesting to ask just how large the mean separations between xanthan molecules are in the solutions under study. Taking anisotropic solutions with concentrations $W = W_a$ as representative and assuming that the molecules are in a regularly spaced, aligned arrangement in the anisotropic phase, the mean interaxial spacing of the aligned X13F3 rods can be estimated to be 51 Å for $C_i = 1.0$ M, 61 Å for $C_i = 0.1$ M, and 73 Å for $C_i = 0.01$ M. Taking the radius of the xanthan double helix to be to be about 11 Å[16] we see that the mean surface-to-surface distance is about 29 Å in the case where $C_i = 1.0$ M. This is significantly greater than the distances at which hydration forces are postulated to dominate the xanthan intermolecular potential, as disclosed by osmotic stress measurements.[84,85] In even the most concentrated anisotropic solution of X13F3 studied here at $C_s = 1.0$ M, the mean surface-to-surface distance is about 16 Å. Isotropic solutions and all of the solutions of X2F2 described in the following paper are less concentrated, so the mean surface-to-surface distance exceeds 20 Å in nearly every case. As the salt concentration is reduced, however, the Debye radius increases rapidly from about 3 Å at $C_s = 1.0$ M to about 10 Å at $C_s = 0.1$ M and 30 Å at $C_s = 0.01$ M. Hence, the *effective radii* of proximate rods overlap significantly for X13F3 solutions with $W \geq W_a$ when $C_s = 0.01$ M and also for X13F3 solutions with $W > W_a$ when $C_s = 0.1$ M. Thus, the influence of salt concentration on the phase behavior of X13F3 and the corresponding rheological changes is easy to rationalize. This issue is discussed further in the companion paper.

Power law analysis of the dependence of the oscillatory shear parameters η^*, G', and G''on W permits one to identify phase boundary concentrations that agree well with the parameters W_i and W_a from phase separation studies in the quiescent solutions (Figures 7 and 8). Moreover, the peak in plots of η against W at small $\dot{\gamma}$ occur very near W_i (Figure 13). This suggests that for larger $\dot{\gamma}$ the peak in η against $\dot{\gamma}$ can be used to identify the onset concentration W_i^{γ} of the biphasic regime at the corresponding shear rate under conditions where the shear field has an influence comparable to the excluded volume effect in provoking a discontinuous increase in the order parameter from the value zero characterizing the isotropic liquid. The effect of steady shear on spontaneous polymer alignment can be seen clearly from Figure 6. At shear rates lower than 50 s^{-1} the peak for $C_s = 1.0$ M appears at $W_i^{\gamma} = 10.05 \approx W_i$, and no shear-induced alignment is observed. When the shear rate is increased to 200 s^{-1}, the peak shifts to $W_i^{\gamma} = 9.49$. Further increase in shear rate to 500 s^{-1} gives a peak viscosity at $W_i^{\gamma} = 8.52$. The shear-induced alignment of this low molecular weight xanthan sample X13F3 is much less significant than observed for the higher molecular weight semiflexible X2F2.[73] Thus, the shear-induced alignment effect appears to be molecular weight dependent with shorter chains requiring higher shear fields to effect alignment than longer chains. For X13F3, the peak in the plot of η vs W persists to the highest accessible shear rates. For X2F2, the peak in plots of η vs W disappears for $\dot{\gamma} \geq 500$ s^{-1}, and it can be concluded that the excluded volume effects are completely dominated by the shear field effect under these conditions for the higher molecular weight polymer.[51]

Acknowledgment. This work was supported by NIH Grant GM 33062. We thank Dr. Theresa M. McIntire for measuring the MWD of samples X2F2 and X13F3 using noncontact AFM.

References and Notes

(1) Jansson, P. E.; Kenne, L.; Lindberg, B. *Carbohydr. Res.* **1975**, *45*, 275−282.

(2) Melton, L. D.; Mindt, L.; Rees, D. A.; Sandersson, G. R. *Carbohydr. Res.* **1976**, *46*, 245−257.
(3) Paradossi, G.; Brant, D. A. *Macromolecules* **1982**, *15*, 874−879.
(4) Sato, T.; Norisuye, T.; Fujita, H. *Macromolecules* **1984**, *17*, 2696−2700.
(5) Stokke, B. T.; Elgsaeter, A.; Smidsrød, O. *Int. J. Biol. Macromol.* **1986**, *8*, 217−225.
(6) Holzwarth, G. *Biochemistry* **1976**, *15*, 4333−4339.
(7) Paoletti, S.; Cesàro, A.; Delben, F. *Carbohydr. Res.* **1983**, *123*, 173−178.
(8) Norton, I. T.; Goodall, D. M.; Frangou, S. A.; Morris, E. R.; Rees, D. A. *J. Mol. Biol.* **1984**, *175*, 371−394.
(9) Sho, T.; Sato, T.; Norisuye, T. *Biophys. Chem.* **1986**, *25*, 307−313.
(10) Liu, W.; Norisuye, T. *Int. J. Biol. Macromol.* **1988**, *10*, 44−50.
(11) Morris, V. J. In *Food Polysaccharides and Their Applications*; Stephen, A. M., Ed.; Marcel Dekker: New York, 1995; Vol. 67, pp 341−375.
(12) Maret, G.; Milas, M.; Rinaudo, M. *Polym. Bull.* **1981**, *4*, 291−297.
(13) Rinaudo, M.; Milas, M. *Carbohydr. Polym.* **1982**, *2*, 264−269.
(14) Milas, M.; Rinaudo, M. *Polym. Bull.* **1983**, *10*, 271−273.
(15) Sato, T.; Kakihara, T.; Teramoto, A. *Polymer* **1990**, *31*, 824−828.
(16) Inatomi, S.-I.; Jinbo, Y.; Sato, T.; Teramoto, A. *Macromolecules* **1992**, *25*, 5013−5019.
(17) Sato, T.; Teramoto, A. *Adv. Polym. Sci.* **1996**, *126*, 85−161.
(18) Sato, T.; Teramoto, A. *Physica A* **1991**, *176*, 72−86.
(19) Dong, X. M.; Kimura, T.; Revol, J.-F.; Gray, D. G. *Langmuir* **1996**, *12*, 2076−2082.
(20) Dong, X. M.; Gray, D. G. *Langmuir* **1997**, *13*, 2404−2409.
(21) Onogi, S.; Asada, T. In *Proceedings of the 8th International Congress on Rheology*; Astarita, G., Marrucci, G., Nicolais, L., Eds.; Plenum: New York, Naples, Italy, 1980; Vol. 1, pp 127−147.
(22) Wissbrun, K. F. *J. Rheol.* **1981**, *25*, 619−662.
(23) Northolt, M. G.; Sikkema, D. J. *Adv. Polym. Sci.* **1990**, *98*, 115−177.
(24) Marrucci, G.; Greco, F. In *Adv. Chem. Phys.*; Prigogine, I., Rice, S. A., Eds.; Wiley: New York, 1993; Vol. 86, pp 331−401.
(25) Mewis, J.; Moldenaers, P. *Curr. Opin. Colloid Interface Sci.* **1996**, *1*, 446−471.
(26) Larson, R. G. *The Structure and Rheology of Complex Fluids*; Oxford University Press: New York, 1999.
(27) Onsager, L. *Ann. N.Y. Acad. Sci.* **1949**, *51*, 627−659.
(28) Flory, P. J. *Proc. R. Soc. London* **1956**, *A234*, 73−89.
(29) Flory, P. J.; Ronca, G. *Mol. Cryst. Liq. Cryst.* **1979**, *54*, 289−310.
(30) Flory, P. J.; Ronca, G. *Mol. Cryst. Liq. Cryst.* **1979**, *54*, 311−330.
(31) Flory, P. J. *Adv. Polym. Sci.* **1984**, *59*, 1−36.
(32) Stroobants, A.; Lekkerkerker, H. N. W.; Odijk, T. *Macromolecules* **1986**, *19*, 2232−2238.
(33) Odijk, T. *Macromolecules* **1986**, *19*, 2313−2329.
(34) Philipse, A. P. *Langmuir* **1996**, *12*, 1127−1133.
(35) Hermans, J., Jr. *J. Colloid Sci.* **1962**, *17*, 638−648.
(36) Kiss, G.; Porter, R. S. *J. Polym. Sci., Polym. Phys. Ed.* **1980**, *18*, 361−388.
(37) Einaga, Y.; Berry, G. C.; Chu, S. G. *Polym. J.* **1985**, *17*, 239−251.
(38) Navard, P. *J. Polym. Sci., Polym. Phys. Ed.* **1986**, *24*, 435−442.
(39) Moldenaers, P.; Mewis, J. *J. Rheol.* **1986**, *30*, 567−584.
(40) Larson, R. G.; Mead, D. W. *J. Rheol.* **1989**, *33*, 185−206.
(41) Moldenaers, P.; Mewis, J. *J. Rheol.* **1993**, *37*, 367−380.
(42) Yan, N. X.; Labes, M. M.; Baek, S. G.; Magda, J. J. *Macromolecules* **1994**, *27*, 2784−2788.
(43) Gillmor, J. R.; Colby, R. H.; Hall, E.; Ober, C. K. *J. Rheol.* **1994**, *38*, 1623−1638.
(44) Walker, L. M.; Wagner, N. J.; Larson, R. G.; Mirau, P. A.; Moldenaers, P. *J. Rheol.* **1995**, *39*, 925−952.
(45) Walker, L. M.; Mortier, M.; Moldenaers, P. *J. Rheol.* **1996**, *40*, 967−981.
(46) Matheson, R. R., Jr. *Macromolecules* **1980**, *13*, 643−648.
(47) Doi, M. *J. Polym. Sci., Polym. Phys. Ed.* **1981**, *19*, 229−243.
(48) Bahar, I.; Erman, B. *J. Polym. Sci., Part B: Polym. Phys.* **1986**, *24*, 1361−1371.
(49) Erman, B.; Bahar, I.; Navard, P. *Macromolecules* **1989**, *22*, 358−364.
(50) Marrucci, G.; Maffettone, P. L. *Macromolecules* **1989**, *22*, 4076−4082.
(51) Marrucci, G. *Rheol. Acta* **1990**, *29*, 523−528.
(52) Larson, R. G. *Macromolecules* **1990**, *23*, 3983−3992.
(53) Larson, R. G.; Doi, M. *J. Rheol.* **1991**, *35*, 539−563.
(54) Sato, T.; Teramoto, A. *Macromolecules* **1991**, *24*, 193−196.
(55) Takada, Y.; Sato, T.; Teramoto, A. *Macromolecules* **1991**, *24*, 6215−6219.
(56) Sato, T.; Takada, Y.; Teramoto, A. *Macromolecules* **1991**, *24*, 6220−6226.
(57) Whitcomb, P. J.; Macosko, C. W. *J. Rheol.* **1978**, *22*, 493−505.
(58) Ross-Murphy, S. B.; Morris, V. J.; Morris, E. R. *Faraday Symp., Chem. Soc.* **1983**, *18*, 115−129.
(59) Cuvelier, G.; Launay, B. *Carbohydr. Polym.* **1986**, *6*, 321−333.
(60) Rochefort, W. E.; Middleman, S. *J. Rheol.* **1987**, *31*, 337−369.
(61) Richardson, R. K.; Ross-Murphy, S. B. *Int. J. Biol. Macromol.* **1987**, *9*, 257−264.
(62) Kojima, T.; Berry, G. C. *Polymer* **1988**, *29*, 2249−2260.
(63) Capron, I.; Brigand, G.; Müller, G. *Int. J. Biol. Macromol.* **1998**, *23*, 215−225.
(64) Oviatt, H. W. J.; Brant, D. A. *Macromolecules* **1994**, *27*, 2402−2408.
(65) Oviatt, H. W. J.; Brant, D. A. *Int. J. Biol. Macromol.* **1993**, *15*, 3−10.
(66) Milas, M.; Reed, W. F.; Printz, S. *Int. J. Biol. Macromol.* **1996**, *18*, 211−221.
(67) Allain, C.; Lecourtier, J.; Chauveteau, G. *Rheol. Acta* **1988**, *27*, 255−262.
(68) Oertel, R.; Kulicke, W.-M. *Rheol. Acta* **1991**, *30*, 140−150.
(69) Jacobs, A.; Kulicke, W.-M. *Macromol. Symp.* **1994**, *84*, 197−207.
(70) Carnali, J. O. *J. Appl. Polym. Sci.* **1991**, *43*, 929−941.
(71) Lim, T.; Uhl, J. T.; Prud'homme, R. K. *J. Rheol.* **1984**, *28*, 367−379.
(72) Santore, M. M.; Prud'homme, R. K. *Carbohydr. Polym.* **1990**, 329−335.
(73) Lee, H.-C.; Brant, D. A. *Macromolecules* **2002**, *35*, 2223.
(74) Van, K.; Asakawa, T.; Teramoto, A. *Polym. J.* **1984**, *16*, 61−69.
(75) Urbani, R.; Brant, D. A. *Carbohydr. Polym.* **1989**, *11*, 169−191.
(76) Talashek, T. A.; Brant, D. A. In *Food Applications*; Millane, R. P., BeMiller, J. N., Chandrasekraran, R., Eds.; Frontiers in Carbohydrate Research 1; Elsevier Applied Science Publishers: London, 1989; pp 271−288.
(77) McIntire, T. M.; Brant, D. A. *Biopolymers* **1997**, *42*, 1334−1146.
(78) Bishay, I. E. Ph.D. Dissertation, University of California, Irvine, 1989.
(79) McIntire, T. M.; Brant, D. A. *J. Am. Chem. Soc.* **1998**, *120*, 6909−6919.
(80) Ferry, J. D. *Viscoelastic Properties of Polymers*; 3rd ed.; John Wiley and Sons: New York, 1980.
(81) Cox, W. P.; Merz, E. H. *J. Polym. Sci.* **1958**, *28*, 619−621.
(82) Itou, T.; Teramoto, A. *Macromolecules* **1988**, *21*, 2225.
(83) Kiss, G.; Porter, R. S. *J. Polym. Sci., Polym. Symp.* **1978**, *65*, 193−211.
(84) Rau, D. C.; Parsegian, V. A. *Science* **1990**, *249*, 1278−1281.
(85) Strey, H. H.; Parsegian, V. A.; Podgornik, R. *Phys. Rev. E* **1999**, *59*, 999−1008.

MA011526M